Irregular timing of population cycles

Jonathan Rubin, David Earn, Priscilla Greenwood, Todd L. Parsons, Karen Abbott

Irregular timing of population cycles

Jonathan E. Rubin[1], David J. D. Earn[2], Priscilla E. Greenwood[3], Todd L. Parsons[4], and Karen C. Abbott[5]

[1]Department of Mathematics, Center for the Neural Basis of Cognition, University of Pittsburgh, Pittsburgh, PA, USA

[2]Department of Mathematics & Statistics, McMaster University, Hamilton, Ontario, Canada

[3]Department of Mathematics, University of British Columbia, Vancouver, British Columbia, Canada

[4]Laboratoire de Probabilités, Statistique et Modélisation (LPSM), Sorbonne Université, CNRS UMR 8001, Paris, France

[5]Case Western Reserve University, Cleveland, Ohio, USA

November 26, 2021

Abstract

Despite considerable study of population cycles, the striking variability of cycle periods in many cyclic populations remains largely unexplained. Mathematical models of cyclic population dynamics seem to exhibit much greater regularity in cycle periods than many real populations, even when accounting for environmental stochasticity. We contend, however, that recent advances in understanding the origins of long transient dynamics point the way to a previously unrecognized means by which environmental stochasticity can create cycle period variation. Specifically, consumer-resource cycles that bring the populations near a saddle point (a combination of population sizes toward which the populations tend, before eventually recovering away) may be subject to a slow passage effect that has been dubbed a saddle crawlby. In this study, we illustrate how stochasticity that generates variability in how close predator and prey populations come to saddles can result in substantial variability in the durations of crawlbys and, as a result, in the periods of population cycles. Our work suggests a new mechanistic hypothesis to explain a significant factor in the irregular timing of population cycles and provides a basis for understanding when environmental stochasticity is, and is not, expected to generate cyclic dynamics with variability across periods.

Introduction

Recurrent population cycles – eruptive increases and crashes in population size – are widespread (Kendall et al. 1999, Barraquand et al. 2017). Consumer-resource and host-enemy interactions are famously known to promote cycles (Turchin and Hanski 2001, Myers 2018), but models of these interactions predict a far more regular cycle period than is observed in many real cyclic populations (Dwyer et al. 2004). The more irregular timing of some cycles is difficult to explain. While it is tempting to implicate environmental stochasticity, the intrinsic period of ecological cycles appears to be surprisingly robust to noise. Past theoretical studies have shown that although white noise readily generates variance in cycle amplitudes, it has little effect on the regularity of the cycle period (Dwyer et al. 2004, Greenman and Pasour 2011). As such, other mechanisms, such as chaos, stochastic transitions between alternative attractors, and resonance between intrinsic cycles and seasonal forcing, have been invoked to explain the irregular timing of some population cycles (Dwyer et al. 2004, Nguyen and Rohani 2007, Ives et al. 2008, Greenman and Pasour 2011, Benincà et al. 2015). These alternative ideas are convincing and no doubt play an important role in some ecological systems. Still, the ubiquity of environmental stochasticity makes it appealing as a parsimonious and perhaps more general explanation for other, unexplained instances of cycle period variability. Though we know from counter-examples (e.g. Dwyer et al. 2004, Greenman and Pasour 2011) that environmental stochasticity *may* not cause significant variance in cycle period, we do not know that it *cannot* cause such variance, so we contend that it deserves a closer look.

In this paper, we reconsider the possibility that the irregular timing of population cycles can originate from the interaction between density-dependent consumer-resource interactions and certain forms of parametric noise, motivated by recent advances in the understanding of ecological transient dynamics (Hastings et al. 2018), which suggest a particular mechanism that may strongly influence cycle timing. In addition to being prone to limit cycles, consumer-resource models generally share another feature: the presence of saddle points at the origin and at the resource carrying capacity in the absence of consumers (Murdoch et al. 2003).

If the consumer-resource cycle brings the population trajectory close enough to these saddle points, then a long transient during which the populations remain near the saddle will result (for an introduction to this role of saddle points, see e.g. Abbott 2020); this effect has been termed a *saddle crawlby* (Hastings et al. 2018). The duration of the crawlby scales with the distance from the saddle (Cushing et al. 1998, Jäger et al. 2008, Morozov et al. 2020). Therefore, we conjecture that stochasticity that results in more variability from cycle to cycle in how close the populations get to these saddles will produce higher variability in cycle timing. To explore this possibility, we partition variance in the total duration of a cycle into variance in the duration of its constituent parts, with particular interest in the times spent passing by and moving between the saddles.

Our contributions come from acknowledging two important features of ecological dynamics. The first is the potential role of saddle crawlbys in cycle period variation. Second, a frustrating problem in population ecology is that there are many different aspects of an underlying ecological process that may be influenced by stochasticity, but different stochastic models can lead to very different dynamics (Allen and Allen 2003, Nisbet and Gurney 2003, Coulson et al. 2004, Vadillo 2019). With this in mind, we seek to understand whether environmental stochasticity in different demographic parameters causes different levels of cycle period variability, and whether any approach the degree of variability seen in real cyclic populations.

In this paper, we study the stochastic Rosenzweig-MacArthur predator-prey model (Rosenzweig and MacArthur 1963) to understand the roles of saddle crawlbys and different sources of environmental noise in generating variably timed population cycles. We find that when stochasticity enters via a parameter that affects how close the cycle passes to saddle points (e.g., the half saturation constant of the predator's functional response), the result is substantial variation in how close the populations come to the saddle points in each cycle, leading to variation in the duration of saddle crawlbys and thus variation in overall cycle period. In contrast, stochasticity in parameters with no direct bearing on the proximity to saddles (e.g., the prey's intrinsic population growth rate) tends to yield much more regular cycles. Our detailed study of the effect of saddle crawlbys on cycle period leads both to a new proposed explanation

for irregularly timed cycles observed in nature and to an understanding of why past work has seen little effect of stochasticity on cycle period variability.

Methods

Basic properties of cyclic populations

While a complete meta-analysis of cycle period variation is well beyond the scope of this study, we do need a reasonable expectation for what levels of variation are realistic. Following Dwyer et al. (2004), we measure cycle period variability by its coefficient of variation (CV). Dwyer et al. (2004) report cycle period CVs ranging from 0.16 to 0.67 for a range of outbreaking forest insects. We supplement these data with our own analysis of ecological time series from the Global Population Dynamics Database (GPDD; NERC Centre for Population Biology 1999). Beginning with the 664 GPDD time series analyzed by Sibly et al. (2007), we found that 459 had at least 2 local maxima and showed some evidence of periodicity (the peak in true wavelet power spectrum exceeded the average observed in 100 bootstrap trials). Of these 459, 47 (10.2 %) showed perfectly regular cycle periods (CV = 0). The remaining cycle period CVs ranged from 0.10 to 0.98. Overall, the cyclic GPDD data had a mean cycle period CV of 0.30. This analysis confirms that the cycle period CVs reported for forest insects in Dwyer et al. (2004) are representative of other taxa as well.

Model formulation

We study cycles in a stochastic version of the Rosenzweig-MacArthur predator-prey model. The underlying deterministic model is

$$\begin{aligned} \frac{dx}{dt} &= rx\left(1-\frac{x}{K}\right)-\frac{axy}{x+h} \\ \frac{dy}{dt} &= \frac{abxy}{x+h}-my, \end{aligned} \tag{1}$$

where x is prey population density and y is predator population density. The prey population grows at maximum rate r and would equilibrate to carrying capacity K in the absence of

predation. Predation occurs according to a Type 2 functional response (Holling 1965) with maximum attack rate a and handling time whose effect is described by the half-saturation constant, h. Predator population growth occurs at a rate proportional (described by b) to its prey consumption rate, and predator death is density independent with rate m.

Our baseline parameter values are listed in Table 1. The implied time unit is most easily interpreted via the mean predator lifetime, which is $1/m \simeq 1.67$ time units. These values result in a limit cycle featuring close, but not too close, passage to the $x = 0$ and $y = 0$ axes and thus to the saddle points of system (1) at $(x, y) = (0, 0)$ and $(K, 0)$. Close passage sets the stage for saddle crawlbys. To enforce a degree of biological realism, though, we omit from our analyses any simulated cycles in which prey and/or predator dropped to very low densities. Although models such as (1) allow recovery from infinitesimally small population densities, we recognize that real populations below a certain size will almost certainly go extinct before recovering. We used 10^{-5} times the prey carrying capacity as the extinction threshold, and chose our baseline parameter set to achieve a low rate of crossing of this threshold unless the noise amplitude was quite high. Imposing this extinction threshold ensures that crawlby effects that we observe in the model are not merely artifacts of letting the system drop to unrealistically low population sizes.

To model different possible ways for environmental stochasticity to affect this interaction, we replace individual parameters with a Cox-Ingersoll-Ross stochastic processes. That is, we make any parameter p (where p is a stand-in for $r, h, \ldots$) stochastic by modeling it as

$$dp = \gamma(\bar{p} - p)dt + \sigma\sqrt{p}\, dW, \tag{2}$$

where W is a Wiener process and $\bar{p}$ is the mean (i.e. baseline) value for the parameter. This formulation prevents parameters from becoming negative and has been shown in past work to have various mathematically desirable and biologically reasonable properties: it is mean-reverting and has a positive temporal autocorrelation that decays exponentially (Allen 2016).

Although we have explored effects of noise in each of the parameters (results not shown), we focus here on contrasting the effects of a noisy prey growth rate, r, versus a noisy predator

handling time, reflected by noise in h. This pair of parameters spans many interesting contrasts (i.e. appearance in a linear versus only in a nonlinear term, a multiplier versus a denominator, a rate in one species' equation versus both) and thus serves well to illustrate the impacts of different sources of noise. We recognize that natural species interactions are not characterized by a single stochastic demographic parameter, but modeling one parameter at a time as stochastic allows us to isolate different putative effects of noise. Modeling noise only in r approximates the situation where the prey's intrinsic growth rate is more sensitive to environmental perturbations (e.g., fluctuations in temperature) than other processes. Noise in h represents a situation where predator behavior or physiology (e.g., digestion rate) is the system feature most sensitive to perturbations.

Analyses

We study our model numerically to answer a series of questions about the genesis of cycle period variation. First, we study the deterministic model (equation (1)) to characterize the impact of different model parameters on the cycle period. We do this by starting with the baseline parameter set and varying one parameter at a time, focusing on each of r and h, to isolate its effect. Although the deterministic model inevitably produces a constant cycle period and we are of course interested in period variability, these results are useful for considering the mechanisms through which noise in specific parameters may impact cycles.

Next, we study the stochastic model (equation (1) in which either r or h varies stochastically according to equation (2)). Specifically, we compute the temporal CV in the simulated cycle periods for different intensities of noise in each of the two parameters. We also partition the cycle into a sequence of six segments (figure 1), **A**: passage by $(0,0)$; **B**: prey growth from near 0 to near K; **C**: passage by $(K,0)$; **D**: predator growth and prey decline (that is, movement from near $(K,0)$ toward the y-axis); **E**: the transition from predator growth to predator decline (i.e. passage across the predator's nullcline); and **F**: finally, sharp predator decline to again approach $(0,0)$. Our hypothesis that saddle crawlbys drive cycle period variability leads us to predict that significant variance should be observed in the passage times near $(0,0)$ and $(K,0)$. We calculate

times spent transitioning through each of the six segments as the populations undergo a cycle, based on times when trajectories cross partition entrance and exit boundaries at locations that we specify in the (x, y) plane. The locations used for these boundaries for most of our simulations are listed in Table B1 in Appendix B; for a few special cases with altered cycle paths (cases 6-9 in Table 2), we used other boundaries. The boundary locations ensure that fluctuations rarely cause spurious crossings, while even those orbits with relatively large fluctuations do not miss any boundaries. Passage times through partition segments are computed sequentially, with the exit boundary from one region also serving as the entrance boundary for the next region (see figure 1). For example, once a trajectory exits a region through its exit boundary, re-entry through the exit boundary due to stochasticity does not count as another passage through the original region; rather, it is ignored, and the calculation of the time of passage through the next region continues until that region's exit boundary is crossed. This subdivision allows us to decompose the variance in the full cycle period based on the variance in the time needed to complete each step.

All of our numerical results on stochastic dynamics represent averages derived from simulations run for 20,000 time units. For each run, we discard an initial period extending from time 0 up until the time of the first crossing of a boundary into any of our defined cycle segments (figure 1). Each sample on which averaging is performed includes at least 400 cycles during which population sizes stay above the extinction threshold.

Two additional analyses supplement our numerical results. First, we used small-noise approximations to derive analytical relationships between certain model features and passage times along the axes and near the saddle points. Due both to their extent and to the innovative mathematics involved, we plan to publish these analytical results elsewhere, but we provide a summary in Appendix A.

Second, in addition to simulations that subjected the deterministic skeleton (1) to environmental noise (2), we investigated the influence of demographic noise. We used the standard Gillespie algorithm (Gillespie 1976, 1977) to recast the system (1),(2) as a continuous-time Markov jump process, whereby exponential holding times alternate with

Markov events (each term in the differential equations (1) is treated as an event rate for changes in the numbers of predators and prey). The degree of demographic stochasticity in the Gillespie simulations is determined by the prey carrying capacity K, which we set to 8000 in all our simulations. To avoid extinctions, we included an additional, small, constant immigration rate (ab); at each immigration event, one predator and $\lceil 1/b \rceil$ prey were added. The time to the next event is drawn from an exponential distribution with mean equal to the inverse of the total rate at which events of any type occur. The probability that the event is of a given type is the ratio of its event rate to the total event rate. The Gillespie simulations are important for confirming that none of our main findings are expected to disappear in the presence of demographic noise and that they are not due simply to specific modeling or methodological choices. We show results from the Gillespie simulations alongside our main numerical results for select, key findings.

Results

Cycle period depends on model parameters and crawlby effects

Depending on the parameter values, the deterministic Rosenzweig-MacArthur model can exhibit a stable equilibrium or a stable limit cycle. Cycles arise when the system undergoes a supercritical Andronov-Hopf (AH) bifurcation, which occurs at $h = h_{AH} := K(ab - m)/(ab + m)$. As h decreases below this threshold, orbits grow quickly from zero amplitude to large cycles that approach the axes in the (x, y) plane (figure 2A-B). Passage along the y-axis corresponds to low levels of prey (x) and declining numbers of predators (y). This is followed by passage near the saddle point at extinction $(0, 0)$, and then by passage along the x-axis in which there are low levels of predators and recovering prey.

Decreasing the prey's growth rate, r, or the predator's half-saturation constant, h, results in longer-period cycles (figure 2C-D, solid black lines). Because the AH bifurcation threshold, h_{AH}, does not involve the parameter r, changing r cannot induce cycles in system (1). Nevertheless, when cycles exist, lowering r lengthens the oscillation period by slowing the recovery of the prey population. This effect prolongs the crawlbys past both the extinction point $(0, 0)$ and the carrying capacity $(K, 0)$ (figure 2C, red dashed and blue dotted lines, respectively). However,

the crawlbys are slowed somewhat less than passage through other parts of the cycle, so the system spends proportionately less time in crawlbys as r decreases (figure 2C, dotted black line in lower panel).

In contrast, reducing h can induce an AH bifurcation and drive the system deeper into the cyclic regime. Decreasing the value of h drives trajectories closer to both axes (figure 2B). This prolongs the two saddle crawlbys (figure 2D, red and blue lines) by placing the populations closer to the saddles. The saddle crawlbys are not only slower with lower h, but they also take up proportionately more of the time needed to complete a cycle (figure 2C, dotted black line).

In sum, slowing the overall dynamics (by decreasing the prey's population growth rate, r) and pushing trajectories closer to the two saddle points (by decreasing the predator's half-saturation constant, h) will each extend the cycle period, but they do so through different mechanisms. Decreasing the prey's growth rate extends the duration of saddle crawlbys, but only by slowing the dynamics as a whole and prolonging the entire cycle period. Decreasing the half-saturation constant enhances the degree to which predators can overexploit their prey, leading to more pronounced population crashes. These crashes exaggerate the crawlby effect by placing the populations closer to the two saddle points at joint extinction and the prey carrying capacity. The result is longer cycles that are made up of relatively more time spent for prey recovery (passage near $(0, 0)$) and then predator recovery (passage near $(K, 0)$).

Stochasticity can cause variance in cycle period, but not all stochasticity is equal

Adding Cox-Ingersoll-Ross parameter noise (equation (2)) to the Rosenzweig-MacArthur model results in noisy cycles such as the ones shown in figure 3. Figure 3A-B shows an example in which noise in r causes cycles to vary in amplitude but maintain a close to constant period. Figure 3C-D shows that for the same noise amplitude (σ value in equation (2)), the cycle period is much more variable for noise in h.

Figure 3 shows just two examples, but they are representative of the systematic differences we found when we explored different intensities of environmental noise acting on different model parameters. For the same absolute noise magnitudes (σ values), the cycle period becomes

much more variable when noise affects handling time than when it affects prey growth rate (figure 4). Specifically, for noise in r, the mean cycle duration changed little with increasing σ from the deterministic value of 24.83 time units, while the standard deviation of these durations depended only weakly on σ (figure 4A). Conversely, mean cycle durations and variability increased substantially with σ when noise entered through h (figure 4B), with a distribution featuring a tail of long cycle durations. For comparison with the biological data (see Methods), note that the results plotted here yield CVs from 0.04 to 0.12 with noise in r and from 0.11 to 0.33 with noise in h. Results for $\sigma = 0.2$ (red bars in figure 4) are also summarized in table 2 (cases 2-3). Finally, if noise enters into both h and r simultaneously (table 2 case 4, implemented via two copies of equation (2) that either share (correlated) or have independent (uncorrelated) instantiations of the Wiener process W), the results are similar to the case with noise in h alone (case 3).

There are several possible explanations for the stronger effect of noise in h than noise in r in generating variable cycle periods. This is the pattern we expect if cycle period variability is driven by variation in the time it takes to complete saddle crawlbys, because changes in h exaggerate the influence of crawlbys while changes in r do not (figure 2C-D). We continue this thread in the next subsection. Alternatively, or perhaps in addition, noise of a particular magnitude may have a larger impact when it enters through h simply because our baseline value of h is lower. In other words, a noise amplitude of, say, $\sigma = 0.2$ acting on an $\bar{r}$ of 1.0 might reasonably have less effect than the same $\sigma = 0.2$ acting on an $\bar{h}$ of 0.15. We tested this idea in two ways. First, we reduced $\bar{r}$ to 0.15 to eliminate the difference in magnitudes between r and h. This results in unrealistically long cycles, but allows a straightforward comparison of standard deviation and CV. Again, the CV in cycle period is much higher when noise enters through h (table 2, cases 6-7). Second, we returned to the baseline parameter set and increased the noise amplitude on r (by rescaling by $\sqrt{h}$) to allow the prey population to become quite small at times, approaching the x-axis and now allowing the exaggerated crawlby effect to be seen via noise in r. The result is a cycle period CV that is now quite comparable to the baseline case with noise in h (table 2, case 5 compared to case 3).

We thus found evidence of true differences (table 2, cases 2-3 and 6-7) in how noise in the prey growth rate and noise in the handling time affect variability in the cycle period. We attribute these differences to the way changes in h affect the relative speed of the crawlbys and investigate this hypothesis in more detail below. We also found evidence that at some sufficiently high level, noise in either parameter can lead to exaggerated crawlbys that cause cycle periods to become more variable (table 2, cases 3 and 5).

Finally, we note that the half-saturation constant, h, is not unique in its ability to drive the system through the AH bifurcation and produce cycles of increasingly large magnitude, as shown in figure 2B; in fact, all parameters except r have that property in this model. Therefore, we consider one more scenario before moving on: we increase m from its baseline value of 0.6 to 0.65. In the absence of stochasticity, this change moves the periodic orbit of the deterministic system (1) from the outer cycle in figure 2A to one of the interior paths. That is, while the system is still cycling with $m = 0.65$, the expected (mean) trajectory does not pass as close to the saddle points. Interestingly, changing m in this way *increases* the variability in cycle periods (figure 5 and table 2, cases 8-9 compared to 2-3). Once again, this effect is particularly strong for handling time noise (table 2). Although we might have expected more cycle period variability deeper into the crawlby region (smaller m), it appears that being closer to the bifurcation – and even on the stable side of it (figure 5D) – may increase the flexibility in the paths that orbits can take. The long durations are still associated with close crawlbys, but crawlbys occur less consistently, leading to a greater mix of longer and shorter cycles. These trends persist with additional increases in m and are reversed by decreases in m (results not shown).

Demographic noise does not overwhelm environmental noise effects

Until now, we have included noise in model (1) as Cox-Ingersoll-Ross parameter noise (equation (2)), representing environmental variability. In reality, population dynamics necessarily include demographic noise as well. In theory, this variability across individuals could induce dynamic effects that dominate the overall cycle paths, reducing the impacts we have documented of environmental fluctuations. We tested this possibility by performing Gillespie simulations (see

Methods) in which all aspects of the population dynamics are treated as events with certain expected rates, and events are implemented sequentially at random, with likelihoods and timings based on these expected rates. These simulations emulate demographic noise effects; moreover, within each simulation, we also modulated either the prey growth rate (r) or the predator's half-saturation constant (h) stochastically. We found that these simulations yielded very similar distributions of cycle durations to our direct simulations of system (1)-(2), matching the differences between noise in r and noise in h as well as those across noise amplitudes σ (figure 4).

Cycle variability is driven by variable passage times near extinction and prey carrying capacity

We have seen that in the deterministic case, trajectories traverse each cycle at non-uniform rates, spending more time near the saddles at $(0,0)$ and $(K,0)$ than in other regions of the phase plane (figure 2A,C,D). This observation raises the question of whether this non-uniformity manifests in the stochastic case and, if so, whether it is relevant for cycle variability. That is, from a naive perspective, longer passage times may translate into more opportunity for fluctuations, resulting in enhanced variability. On the other hand, we have seen (from the contrast in simulations with noisy r versus noisy h) that longer passage times do not inevitably result in variable cycle periods. Moreover, it is also possible that the strong contraction near the stable manifold of each saddle could constrain trajectories, and hence passage times, to be more similar rather than more variable, relative to what occurs in other regions of phase space.

As the noise amplitude σ increases, trajectories continue to spend significant portions of each cycle near the $(0,0)$ and $(K,0)$ saddles, although the precise locations where this time is spent become progressively more diverse (figure 6 shows this for noise in r; the effect is similar but not shown for noise in h). In fact, by comparing plots with no noise to those with $\sigma \geq 0.2$, it appears that with increasing σ, trajectories spend relatively less time transitioning from the neighborhood of $(K,0)$ back to the neighborhood of the y-axis, although it is not obvious by inspection where that time is spent instead.

To quantify these effects, we used linear sections to partition the part of the phase plane

visited by the stochastic trajectories into six disjoint regions, proceeding counterclockwise as follows (figure 1), **A**: neighborhood of the origin, **B**: passage along the x-axis, **C**: neighborhood of the $(K, 0)$ saddle, **D**: passage along the unstable manifold of $(K, 0)$, which defines the direction in which trajectories depart from the neighborhood of $(K, 0)$, **E**: crossing of the y-nullcline, which is the curve where dy/dt switches from positive to negative, and **F**: passage along the y-axis. The distributions of times spent in these regions differ significantly in their variability (figure 7). By a clear margin, the most variability arises in the passage times through regions **A** and **C**, corresponding to crawlbys near the saddles. Moreover, substantially more variability occurred in these regions with noise in h than with noise in r; note the differences in x-axis details between histograms in figure 4A,C and those in figure 4B,D. The Gillespie simulations shown in figure 4C,D yielded qualitatively, and in many cases quantitatively, similar results (tables 3, 4).

Although the variability in the durations of the crawlbys (that is, in passage times near $(0, 0)$ and $(K, 0)$) becomes substantial, these segments of each cycle still dominate the overall cycle period. For example, the positive correlation between period and these passage times, but not between period and passage time along the x-axis, is readily apparent in figure 8. Interestingly, these relationships, especially for the passage time near $(0, 0)$, are even tighter with noise in r than with noise in h, although the passage times themselves are less widely distributed when the noise is in r.

Loss of prey strongly influences each cycle period, with little history dependence between cycles

So far, we have shown strong evidence that environmental noise has different impacts on the distribution of cycle periods, depending on the origin of the noise, and that variability in cycle periods is dominated by variability in the duration of the two saddle crawlbys near $(0, 0)$ and $(K, 0)$. To conclude our characterization of these effects, we ask what factors best predict these crawlby durations. Longer crawlbys elevate the risk of stochastic extinction by prolonging the time during which one or both populations are small. Longer crawlbys also delay the time until the next population peak, with important consequences for some cyclic species like outbreaking

forest insects. We therefore ask, what should we look for in a population's history to help us anticipate the durations of upcoming saddle crawlbys?

In a deterministic system, passage time near a saddle is well understood. We can consider the population trajectory to have started the crawlby past extinction (that is, to have entered the neighborhood of the $(0,0)$ saddle) once predator density, y, drops below some threshold, $y_{0,\text{in}}$. Suppose the prey density when the $y = y_{0,\text{in}}$ threshold is crossed is $x_{0,\text{in}}$. We will say the $(0,0)$ crawlby is complete once prey density grows beyond another threshold, $x_{0,\text{out}}$. Near $(0,0)$, $x^2 \approx 0$ and $xy \approx 0$, so the dynamics of the deterministic Rosenzweig-MacArthur model (equation (1)) is well approximated by $dx/dt = rx$, $dy/dt = -my$. In this approximation, the time needed to complete the saddle crawlby is $t_{pass} = (1/r)\ln(x_{0,\text{out}}/x_{0,\text{in}})$; that is, the crawlby duration depends linearly on $\ln(x_{0,\text{in}})$. A similar calculation implies that the log predator density at entry into the neighborhood of the $(K,0)$ saddle, $y_{K,\text{in}}$, also depends linearly on $\ln(x_{0,\text{in}})$.

If the relationships for the deterministic model still hold in the presence of environmental stochasticity, then we expect $\ln(x_{0,\text{in}})$, the log prey density when the populations first enter the vicinity of the extinction state $(0,0)$, to predict the duration of both saddle crawlbys. This is indeed what we find. There is a strong correlation between $\ln(x_{0,\text{in}})$ and the passage time by the $(0,0)$ saddle (figure 9A,B). There is also a strong correlation between log prey density, $\ln(x_{0,\text{in}})$, and log predator density upon entry into the neighborhood of the $(K,0)$ saddle (figure 9C,D), and between the time of passage near $(K,0)$ and this log predator density (figure 9E,F). Thus, even in the presence of noise, the prey's population density at the end of the predator-decline portion of the cycle strongly influences the durations of both saddle crawlbys, which in turn strongly influence the time it will take to complete the current cycle.

The effects of noise during the passage around the rest of the cycle eliminates the effects of these entry positions, so that the positions of entry into the neighborhoods of the saddles in the next cycle are effectively independent of past history (Appendix B, figure B1). This means that we expect no meaningful autocorrelation in the periods of consecutive cycles. It also validates our decision (see Methods) to omit individual cycles with unrealistically low population sizes

from our analyses. The consistency of Gillespie simulation results with those from simulating (1)-(2) provides additional evidence that successive cycles are effectively independent.

Finally, referring back to Figure 9 and comparing the two columns, we notice that the predator and prey densities upon entry into the two saddle neighborhoods differ, depending on the source of noise. When noise enters through the prey's population growth rate, r, the entry values seem to be symmetrically distributed on the logarithmic scale, while when noise enters through the handling time, they become skewed toward smaller values even on the logarithmic scale, corresponding to the skew toward longer passage times (figures B2-B3). Interestingly, both patterns of entry densities correspond well to a lognormal distribution function. This suggests a characteristic distribution of densities upon approach to a saddle in this model, with moments that depend on the source of the noise.

Discussion

Although real cyclic populations can display considerable variability in cycle period, previous authors have observed that stochastic ecological models typically predict cycles with much more regular periods (Dwyer et al. 2004, Greenman and Pasour 2011). Inspired by recent work characterising saddle crawlbys in non-equilibrium ecological dynamics (Hastings et al. 2018), we hypothesized that stochasticity that causes variation in how close populations come to saddle points during their cycles might promote variability in cycle periods. Our numerical study of stochastic Rosenzweig-MacArthur predator-prey cycles confirms this idea. For the cycles that we observe in model simulations, variability in period is dominated by deviation in the passage times past the saddle points (figures 7, 8); further evidence for the central impact of saddle crawlbys arises in the scaling of these passage times with proximity to the stable manifolds of the two saddles (i.e. the x- and y-axes; figure 9). Our results thus update our understanding of the conditions under which environmental stochasticity can contribute meaningfully to observed cycle period variation in nature.

Within this qualitatively general phenomenon of crawlby-induced variability, quantitative differences arise depending on the source and amplitude of the stochasticity in the dynamics of

population interactions. Comparing deviations of similar amplitude, we find that handling time noise, which causes variation in the efficiency with which predators exploit their prey and hence in the extent of the population crashes experienced on each passage around the cycle, induces more variability in cycle period than does noise in the prey's population growth rate (figures 3, 4, 7; Table 2, cases 2-3). Rescaling our noise sources to equalize the CV of the fluctuations from these sources, rather than their amplitude, seems to mitigate this difference (Table 2, case 3 vs. case 5). Yet, when we vary parameters to induce closer passage near the axes and saddles, corresponding to more extreme population losses during cycle troughs, and also to equalize the noise source CVs, the difference between these noise sources re-emerges (Table 2, case 6 vs. case 7). A heuristic idea of the cause of this distinction comes from the observation that for fixed predator level y, noise in r enters the dynamic equation for x in equation (1) in a linear manner, with small deviations in r multiplying the small term $x(1 - x/K) \sim x$ near $x = 0$. On the other hand, noise in h enters the equations like $1/h$, such that even small deviations in h can have an amplifying effect (Appendix A).

Another quantitative, and perhaps initially surprising, observation emerging from our study is that crawlby-induced variability is strongest when the mean cycle trajectory is not too close to the saddle points (figures 2A, 5), such that individual cycles represent a mix of crawlbys and non-crawlbys. Indeed, even though crawlbys are responsible for the overall cycle duration variability, the most heterogeneous mixture of long and short passage times past saddles results when crawlbys are only influential on a subset of cycles. In these cases, the coefficient of variation in cycle period approaches 0.3, the mean value estimated from GPDD data. We therefore conclude that variance in the duration of saddle crawlbys provides a viable explanation for some, although not all, observed instances of variability in cycle periods. This result also highlights the point that even though cyclic populations do not come close to extinction during several consecutive cycles, their population dynamics may hold the ingredients to produce significant crashes under environmental fluctuations that are within the range of expected occurrence.

Like any model, ours is not a complete representation of reality. Real predators may

disperse, change behaviors, or evolve to avoid driving their prey, and thus themselves, too close to extinction (van Baalen and Sabelis 1995). Alternatively, in biological systems, local populations with high-amplitude cycles may routinely go extinct and then undergo recolonization. Our results were conditioned on the populations not going extinct, and we do not model dispersal in or out of the local community nor do we model complex behaviors, alternative prey, and other such factors that are likely to influence the dynamics of real populations. Nevertheless, the elements of our model, like population cycles and saddle crawlbys, and their connections to real dynamics are well studied (Murdoch et al. 2003). Our contribution, therefore, is not to replicate or explain the dynamics of any specific single population, but to extend our understanding of cycles and crawlbys as mechanisms through which environmental stochasticity can emerge within predator-prey dynamics in general. In doing so, we reconcile a long-recognized mismatch between models and data in their view of how variable the periods of cycle populations may be.

Because populations necessarily become small during the trough of each cycle, one might reasonably expect demographic stochasticity to be important in this setting. However, our Gillespie simulations reveal that the effects of environmental stochasticity on cycle period variation are robust to the inclusion of demographic noise. It is nevertheless possible that other dynamic mechanisms not considered in this study may also contribute to temporal variability in cycle durations. Our intent is not to argue that saddle crawlbys are the only or even the predominant source of cycle period variability, but rather to highlight their putative role.

The observations in this paper represent interesting topics for future mathematical analysis, particularly for models such as (1)-(2) to which the stochastic averaging methods of Skorokhod et al. (2002) cannot be applied. Previous analytical and numerical work, some done in other biological contexts, has discussed some of the differences in dynamics that arise from the details of how stochasticity appears in a dynamical system (Lande 1993, Goldwyn and Shea-Brown 2011, Allen 2016, Vadillo 2019). In contrast to the individual-level impact of demographic noise, environmental noise is shared across entire populations, which is conducive to larger variability and can increase the likelihood of extreme events such as extinction (Lande 1993). The specific

representation of stochasticity that we have implemented in equation (2) features biologically desirable properties: it causes the stochastic parameter to remain positive, to be mean-reverting, and to have some history-dependence, with a temporal autocorrelation that is nonzero and decays exponentially (c.f. Allen 2016). To our knowledge, analytical work to date has not addressed how such stochasticity impacts cycle durations and other properties in systems with saddle crawlbys. A related direction that has been pursued analytically (Ashwin and Postlethwaite 2016) is how stochasticity affects the passage of trajectories along a heteroclinic cycle (i.e., a union of orbits that each form a connection from one saddle point to another, which together form a closed loop). These systems may require noise to oscillate, unlike model (1), but nonetheless the resulting oscillations do feature passage near saddle points. Ashwin and Postlethwaite (2016) analyzed residence times near equilibria and switches between neighborhoods of attractors (including heteroclinic cycles), while Giner-Baldó et al. (2017) derived analytical approaches to compute the power spectra of observables in a planar system with a heteroclinic cycle. Both of these analyses were done on systems with stochasticity in the form of additive Gaussian white noise, however, whereas the CIR noise that we consider poses a new challenge for future work.

Our results update our understanding of how environmental stochasticity can contribute meaningfully to observed cycle period variation in nature. While our results for stochastic prey growth rate, r, largely confirm past results that stochasticity has little effect on cycle period, we have shown that some noise sources – specifically those that vary the distance from saddle points as part of the normal cycle – can lead to substantial cycle period variation. Interestingly, this effect is strongest when the mean cycle trajectory is not too close to the saddle points, such that individual cycles represent a mix of crawlbys and non-crawlbys. In these cases, the coefficient of variation in cycle period approached 0.3, the mean value estimated from time series data. We therefore conclude that variance in the duration of saddle crawlbys provides a viable explanation for some, though not all, observed instances of variability in cycle periods.

Literature Cited

Abbott, K. C. 2020. Non-equilibrium dynamics and stochastic processes. Pages 40–52 *in* K. S. McCann and G. Gellner, eds. Theoreitcal Ecology: Concepts and Applications. Oxford University Press.

Allen, E. 2016. Environmental variability and mean-reverting processes. DCDS-B 21:2073–2089.

Allen, L. J. S., and E. J. Allen. 2003. A comparison of three different stochastic population models with regard to persistence time. Theoretical Population Biology 64:439–449.

Ashwin, P., and C. Postlethwaite. 2016. Quantifying noisy attractors: From heteroclinic to excitable networks. SIAM Journal on Applied Dynamical Systems 15:1989–2016.

Barraquand, F., S. Louca, K. C. Abbott, C. A. Cobbold, F. Cordoleani, D. L. DeAngelis, B. D. Elderd, J. W. Fox, P. Greenwood, F. M. Hilker, et al. 2017. Moving forward in circles: challenges and opportunities in modelling population cycles. Ecology letters 20:1074–1092.

Benincà, E., B. Ballantine, S. P. Ellner, and J. Huisman. 2015. Species fluctuations sustained by a cyclic succession at the edge of chaos. Proc Natl Acad Sci USA 112:6389–6394.

Coulson, T., P. Rohani, and M. Pascual. 2004. Skeletons, noise and population growth: the end of an old debate? Trends in Ecology and Evolution 19:359–364.

Cushing, J. M., B. Dennis, R. A. Desharnais, and R. F. Costantino. 1998. Moving toward an unstable equilibrium: saddle nodes in population systems. Journal of Animal Ecology 67:298–306.

Dwyer, G., J. Dushoff, and S. H. Yee. 2004. The combined effects of pathogens and predators on insect outbreaks. Nature 430:341–345.

Gillespie, D. T. 1976. A general method for numerically simulating the stochastic time evolution of coupled chemical reactions. Journal of Computational Physics 22:403–434.

———. 1977. Exact stochastic simulation of coupled chemical-reactions. Journal Of Physical Chemistry 81:2340–2361.

Giner-Baldó, J., P. J. Thomas, and B. Lindner. 2017. Power spectrum of a noisy system close to a heteroclinic orbit. Journal of Statistical Physics 168:447–469.

Goldwyn, J. H., and E. Shea-Brown. 2011. The what and where of adding channel noise to the hodgkin-huxley equations. PLoS Comput Biol 7:e1002247.

Greenman, J. V., and V. B. Pasour. 2011. Journal of Theoretical Biology. J Theor Biol 278:74–86.

Hastings, A., K. C. Abbott, K. M. Cuddington, T. Francis, G. Gellner, Y.-C. Lai, A. Morozov, S. Petrovskii, K. Scranton, and M. L. Zeeman. 2018. Transient phenomena in ecology. Science 361:eaat6412.

Holling, C. S. 1965. The functional response of predators to prey density and its role in mimicry and population regulation. Memoirs of the Entomological Society of Canada 97:5–60.

Ives, A. R., Á. Einarsson, V. A. A. Jansen, and A. Gardarsson. 2008. High-amplitude fluctuations and alternative dynamical states of midges in Lake Myvatn. Nature 452:84–87.

Jäger, C. G., S. Diehl, C. Matauschek, C. A. Klausmeier, and H. Stibor. 2008. Transient dynamics of pelagic producer-grazer systems in a gradient of nutrients and mixing depths. Ecology 89:1272–1286.

Kendall, B. E., C. J. Briggs, W. W. Murdoch, P. V. Turchin, S. P. Ellner, E. McCauley, R. M. Nisbet, and S. N. Wood. 1999. Why do populations cycle? A synthesis of statistical and mechanistic modeling approaches. Ecology 80:1789–1805.

Lande, R. 1993. Risks of population extinction from demographic and environmental stochasticity and random catastrophes. Am Nat 142:911–927.

Morozov, A., K. C. Abbott, K. M. Cuddington, T. Francis, G. Gellner, A. Hastings, Y.-C. Lai, S. Petrovskii, K. Scranton, and M. Lou Zeeman. 2020. Long transients in ecology: Theory and applications. Physics of Life Reviews 32:1–40.

Murdoch, W. W., C. J. Briggs, and R. M. Nisbet. 2003. Consumer-Resource Dynamics. Princeton University Press.

Myers, J. H. 2018. Population cycles: generalities, exceptions and remaining mysteries. Proceedings of the Royal Society B: Biological Sciences 285:20172841.

NERC Centre for Population Biology. 1999. The Global Population Dynamics Database. Imperial College, London.

Nguyen, H. T. H., and P. Rohani. 2007. Noise, nonlinearity and seasonality: the epidemics of whooping cough revisited. J Roy Soc Interface 5:403–413.

Nisbet, R. M., and W. C. S. Gurney. 2003. Modelling Fluctuating Populations. Blackburn Press.

Rosenzweig, M. L., and R. H. MacArthur. 1963. Graphical representation and stability conditions of predator-prey interactions. American Naturalist pages 209–223.

Sibly, R. M., D. Barker, J. Hone, and M. Pagel. 2007. On the stability of populations of mammals, birds, fish and insects. Ecology Letters 10:970–976.

Skorokhod, A. V., F. C. Hoppensteadt, and H. Salehi. 2002. Random perturbation methods with applications in science and engineering. Springer.

Turchin, P. V., and I. Hanski. 2001. Contrasting alternative hypotheses about rodent cycles by translating them into parameterized models. Ecol Lett 4:267–276.

Vadillo, F. 2019. Applied Mathematics and Computation. Applied Mathematics and Computation 360:181–189.

van Baalen, M., and M. W. Sabelis. 1995. The milker-killer dilemma in spatially structured predator-prey interactions. Oikos 74:391–400.

Tables

Table 1. Baseline parameters of the model defined by equations (1) and (2).

parameter	meaning	value	unit
r	prey intrinsic growth rate	1	time^{-1} *per capita*
K	prey carrying capacity	1	prey biomass
a	maximum prey consumption rate	2	time^{-1} per predator
h	prey density at half maximum consumption rate	0.15	prey
b	prey to predator conversion efficiency	0.5	—
m	predator death rate	0.6	time^{-1} *per capita*
p	parameter subject to CIR process (r or h)		
γ	speed of adjustment to mean $\bar{p}$	1	time^{-1}
σ	$\sigma\sqrt{p}$ is standard deviation of CIR process	0–0.3	$\sqrt{\text{units of } p}$

For stochastic r or h, the values listed refer to $\bar{r}$ or $\bar{h}$, respectively.

Table 2. Mean, standard deviation, and coefficient of variation of cycle periods under different scenarios.

case	noise site	parameter set	noise amplitude, σ	mean period	standard deviation	CV
1	none	baseline	0 (deterministic)	24.83	0	0
2	r	baseline	0.2	24.74	2.07	0.084
3	h	baseline	0.2	28.88	5.59	0.19
4 (uncorr)	r and h	baseline	$\sigma_r = \sigma_h = 0.2$	28.70	5.47	0.19
4 (corr)	r and h	baseline	$\sigma_r = \sigma_h = 0.2$	29.76	6.01	0.20
5	r	baseline	$0.2/\sqrt{\bar{h}} = 0.516$	25.26	5.06	0.20
6	r	$\bar{r} = \bar{h} = 0.15$	0.2	68.04	4.30	0.063
7	h	$\bar{r} = \bar{h} = 0.15$	0.2	61.81	7.58	0.123
8	r	$m = 0.65$	0.2	23.79	2.30	0.097
9	h	$m = 0.65$	0.2	28.95	7.80	0.27

Our baseline parameter set given in Table 1 is used except where noted. With the exception of the deterministic case, either r or h (or both in case 4 where uncorr refers to uncorrelated, corr to correlated; see text) is made stochastic by applying equation (2).

Table 3. Mean (μ) and standard deviation (sd) of passage times through regions **A**-**F** (see figure 1) from model (1)-(2) (SDE) simulations.

noise site	noise amp., σ	μ_A	sd_A	μ_B	sd_B	μ_C	sd_C	μ_D	sd_D	μ_E	sd_E	μ_F	sd_F
r	0.1	4.34	0.32	2.59	0.14	9.32	0.69	3.31	0.07	2.95	0.11	2.19	0.05
r	0.2	4.34	0.68	2.61	0.29	9.32	1.49	3.31	0.15	2.95	0.25	2.21	0.13
r	0.3	4.43	0.98	2.64	0.48	9.52	2.12	3.30	0.22	2.92	0.41	2.24	0.29
h	0.1	6.34	0.98	1.49	0.09	11.07	2.53	2.77	0.25	2.75	0.15	1.32	0.15
h	0.2	7.36	2.10	1.51	0.24	13.19	5.21	2.76	0.48	2.70	0.34	1.36	0.47
h	0.3	8.13	2.63	1.64	1.54	14.52	6.21	2.80	0.84	2.57	0.43	1.45	0.76

Table 4. Mean (μ) and standard deviation (sd) of passage times through regions **A**-**F** (see figure 1) from Gillespie simulations.

noise site	noise amp., σ	μ_A	sd_A	μ_B	sd_B	μ_C	sd_C	μ_D	sd_D	μ_E	sd_E	μ_F	sd_F
r	0.1	4.34	0.57	2.61	0.18	9.22	1.91	3.31	0.24	2.96	0.16	2.21	0.12
r	0.2	4.35	0.78	2.62	0.31	9.25	2.18	3.30	0.28	2.95	0.26	2.23	0.16
r	0.3	4.34	1.11	2.67	0.48	9.15	2.58	3.33	0.98	2.93	0.37	2.27	0.60
h	0.1	6.31	1.15	1.50	0.11	10.80	3.06	2.78	0.32	2.76	0.18	1.33	0.19
h	0.2	6.95	1.80	1.55	0.77	11.77	4.23	2.75	0.52	2.72	0.32	1.36	0.42
h	0.3	7.69	2.01	1.65	1.79	13.22	4.96	2.76	1.39	2.62	0.44	1.51	1.37

Figure legends

Figure 1. Components of a typical cycle, **A**: passage by the origin when both species are rare, **B**: recovery of the prey population, **C**: passage by the prey's carrying capacity, K, **D**: predator recovery and prey decline, **E**: initiation of predator decline, and finally **F**: sharp predator decline back toward the origin. Segments **A** and **C** involve saddle crawlbys.

Figure 2. Oscillations in system (1) without noise. **A**. The predator-prey coexistence equilibrium is unstable for $h \lesssim 0.25$ and baseline values of the other parameters. Periodic orbits for successively smaller values of h, namely $h = 0.24$ (diamonds), $h = 0.195$ (circles), and $h = 0.15$ (squares; our baseline value) pass progressively closer to the coordinate axes. Shapes denote points 1 time unit apart on each orbit and thus show the rates of passage through different parts of the cycle. **B**. As h is reduced from 0.4 toward its baseline value (0.15), system (1) undergoes an Andronov-Hopf bifurcation at which the coexistence equilibrium switches from stable (solid black) to unstable (dashed black) and a family of stable periodic orbits emerges (blue and red show maximal and minimal values of x and y, respectively, along these orbits). **C**. As r (baseline value 1.0) decreases, the oscillation period grows (solid black line). This is partially explained by prolonged crawlbys past the saddles at $(0, 0)$ (blue dotted line) and $(K, 0)$ (red dashed line). The purple dashed line shows the total amount of time during each cycle that is spent in a saddle crawlby (red plus blue), and the dotted black line in the lower panel shows the remaining time spent passing through other parts of the cycle (solid black minus purple). **D**. As h decreases, the oscillation period grows, but less extremely than in **C**. The longer cycle duration is even more strongly influenced by saddle crawlbys; for low h, most of the time needed to complete a cycle is spent crawling by the saddle points.

Figure 3. Typical behavior of system (1)-(2) with noise amplitude $\sigma = 0.3$ and noise in r (**A-B**) or h (**C-D**). **A, C** show the dynamics over 2000 time units in the (x, y) phase plane. **B, D** show time series of x (black) and y (red) for the first 500 of the 2000 time units shown in **A, C**.

Figure 4. Distributions of relative cycle durations for various noise amplitudes σ. **A-B**. Results

from simulations with model (1),(2). **A**. With noise in r, the mean duration stays nearly constant while the distribution widens and remains symmetric as σ increases. **B**. With noise in h, the mean duration increases and the distribution widens and becomes skewed, with a tail of long duration cycles, as σ increases. Note that the two panels show different ranges of cycle durations. **C-D**. Results from Gillespie simulations of model (1) with carrying capacity $K = 8000$ and environmental noise in r (**C**) or in h (**D**) are similar to those from the simulations with *only* environmental noise shown in **A, B**. These plots were derived from equal time simulations across noise conditions, which led to the following numbers of cycles. For the Gillespie case: $\sigma_h = 0.1$, 978 cycles; $\sigma_h = 0.2$, 915 cycles; $\sigma_h = 0.3$, 839 cycles; $\sigma_r = 0.1$, 1018 cycles; $\sigma_r = 0.2$, 1018 cycles; $\sigma_r = 0.3$, 1003 cycles. For simulations of (1), (2): $\sigma_h = 0.1$, 775 cycles; $\sigma_h = 0.2$, 668 cycles; $\sigma_h = 0.3$, 410 cycles; $\sigma_r = 0.1$, 809 cycles; $\sigma_r = 0.2$, 808 cycles; $\sigma_r = 0.3$, 798 cycles.

Figure 5. Time series for **A**: $m = 0.6$, **B**: $m = 0.65$, **C**: $m = 0.7$, and **D**: $m = 0.75$ with noise of amplitude $\sigma = 0.2$ in h. The system undergoes an Andronov-Hopf bifurcation at $m \in (0.7, 0.75)$. Thus, the deterministic model would show limit cycles for the parameter values in **A-C** and stable predator-prey coexistence for the values in **D**.

Figure 6. Histograms of relative times spent in bins in the (x, y) plane during simulations with durations of 2000 time units, with **A** no noise and with **B-D** increasing levels of noise amplitude σ. These results are for noise in the prey carrying capacity r, and are similar to what we see with noise in the predator's half-saturation constant h.

Figure 7. Histograms of time spent by trajectories with noise of amplitude σ in r (top plot per pair) or in h (bottom) in successive regions of phase space, **A**: near the origin, **B**: along the x-axis, **C**: near the $(K, 0)$ saddle point, **D**: along the unstable manifold of $(K, 0)$, **E**: traversing the y-nullcline, **F**: along the y-axis. For noise in h, note that the distributions in regions **B** and **F** have sharp minima corresponding to the passage times generated by $dx/dt = rx(1 - x/K)$ and $dy/dt = -my$, respectively, which are approached on cycles for which the stochastic xy term (the functional response) becomes so small that it has very limited influence over the passage times along the axes. The numbers of cycles incorporated in these histograms are as in Figure 4.

Figure 8. Correlations between the different durations for **A-B**: noise in the prey growth rate (r) or **C-D**: noise in the handling time (implemented as noise in the predator's half-saturation constant, h) for baseline parameter values and noise amplitude $\sigma = 0.2$. **A,C**. The full cycle period (per) is tightly correlated with passage times near the $(0,0)$ and $(K,0)$ saddle points (blue triangles and red circles, respectively). In contrast, it is effectively independent of the time it takes to transition between the saddles ("x-axis passage", cyan markers). Here, noise is applied with $\sigma = 0.2$ in all cases. **B,D**. Cycle period is highly correlated with the total time needed to complete both saddle crawlbys ("sum", black dots). It is uncorrelated with the time needed to complete all other parts of the cycle ("difference", i.e. the total cycle period minus the sum of the two saddle crawlby durations; green dots).

Figure 9. Strong dependence of passage times through saddle neighborhoods on entry positions into those neighborhoods. In **A,C,E** the prey growth rate, r, is the stochastic parameter and in **B,D,F** the predator's prey handling time, h, is stochastic. **A-B** show the dependence of the $(0,0)$ saddle crawlby duration on the log of the prey's density upon entry into that neighborhood, $(\ln(x_{0,\text{in}}))$. **C-D** show dependence of log predator density upon entry into the neighborhood of $(K,0)$, $(\ln(y_{K,\text{in}}))$, on $\ln(x_{0,\text{in}})$. Finally, **E-F** show how $\ln(y_{K,\text{in}})$ determines the duration of the $(K,0)$ saddle crawlby. Results for noise amplitude $\sigma = 0.1$, 0.2 and 0.3 are shown in **A,B,E,F**, while **C,D** show $\sigma = 0.2$.

616

Figures

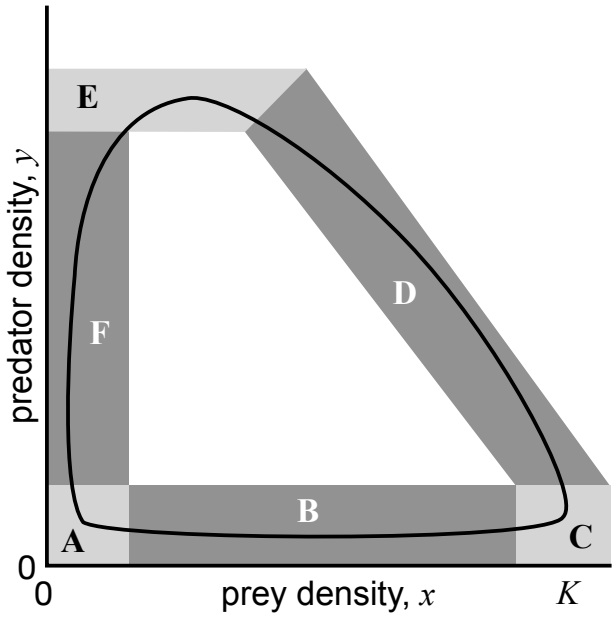

Figure 1

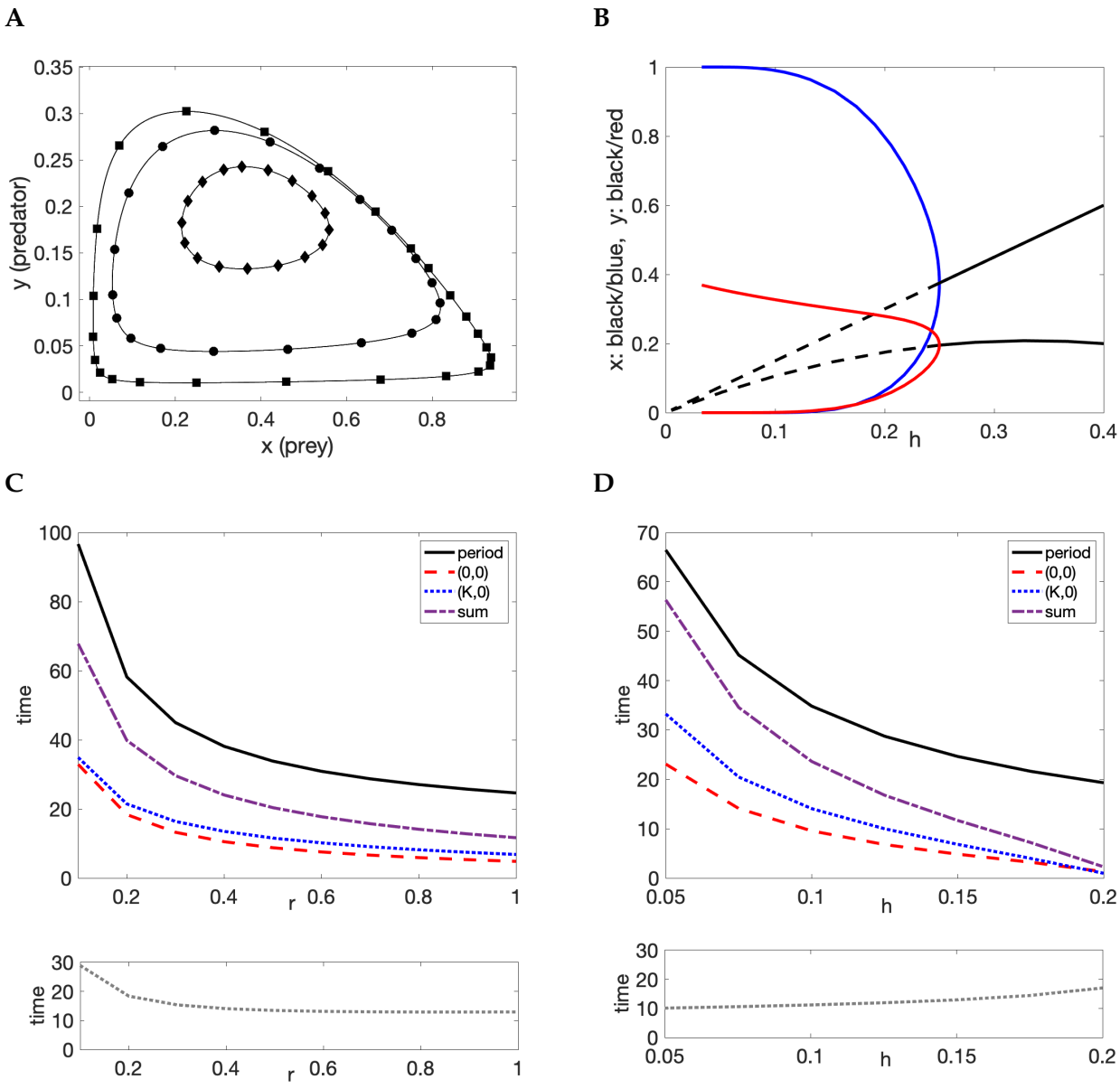
A
B
C
D
y (predator)
x (prey)
x: black/blue, y: black/red
h
time
r
period
(0,0)
(K,0)
sum

Figure 2

A. Noise in r

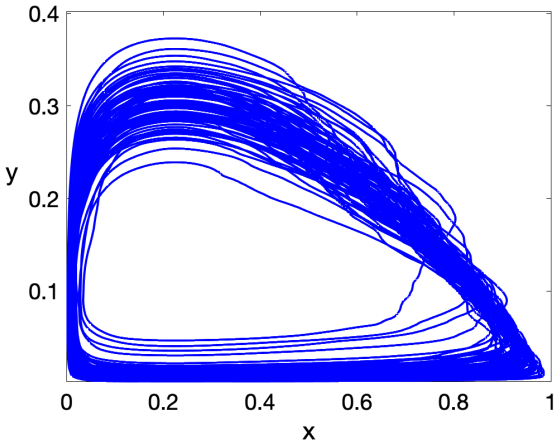

B. Noise in r

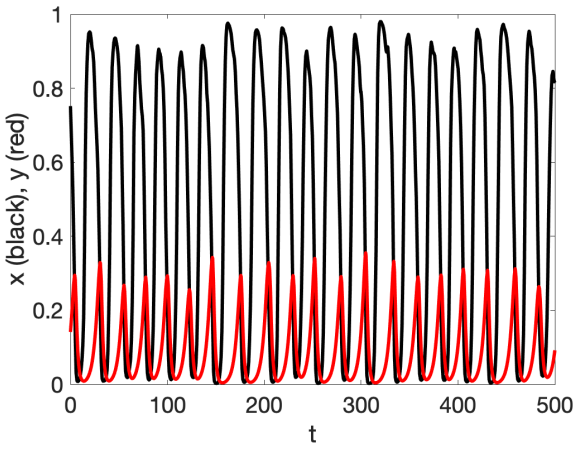

C. Noise in h

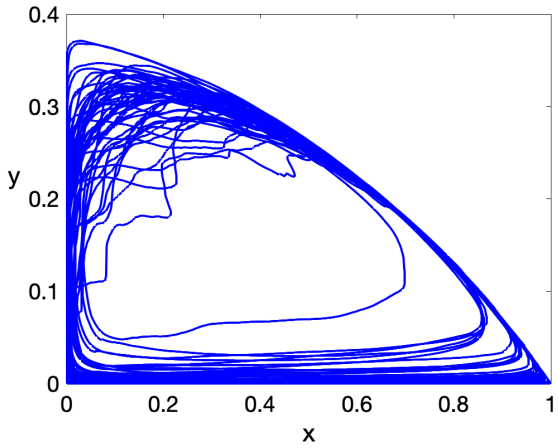

D. Noise in h

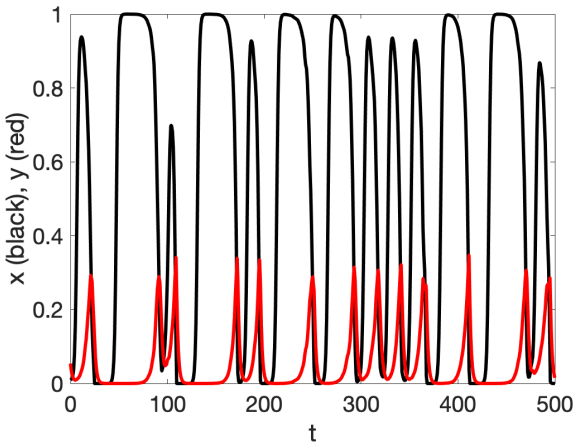

Figure 3

A. Noise in r, Eqns (1)-(2)

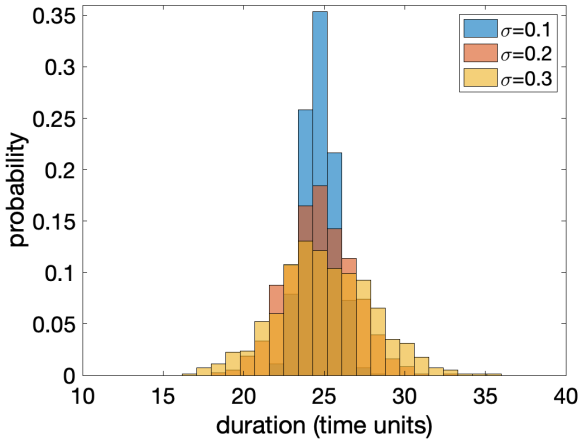

B. Noise in h, Eqns (1)-(2)

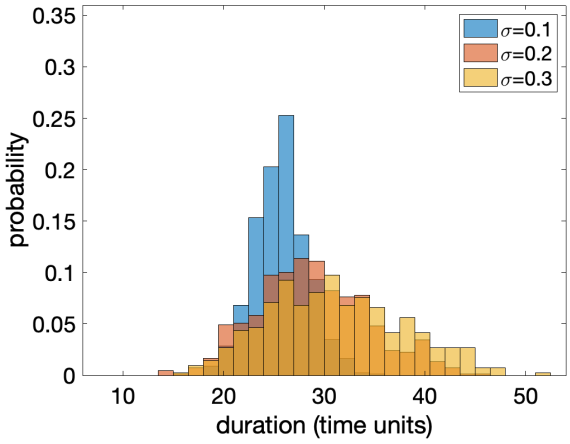

C. Noise in r, Gillespie algorithm

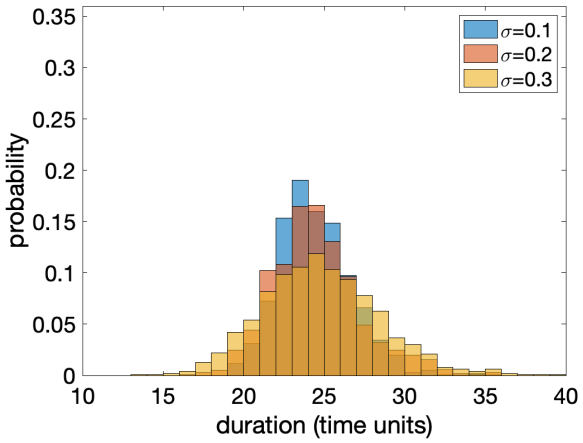

D. Noise in h, Gillespie algorithm

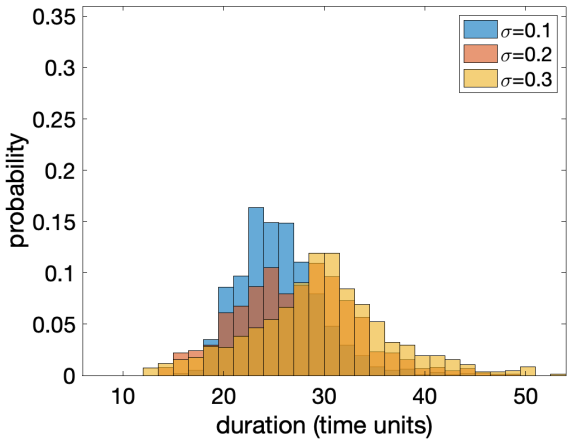

Figure 4

A. $m = 0.6$

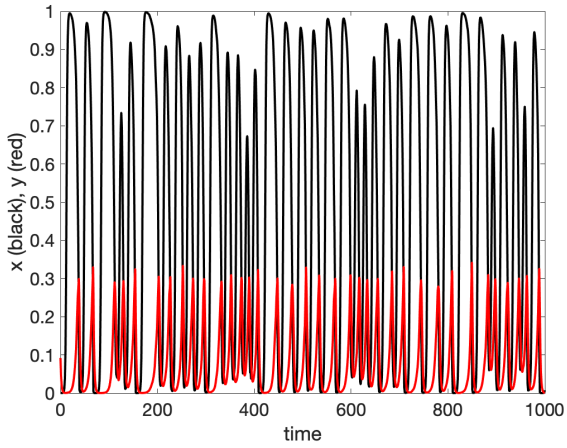

B. $m = 0.65$

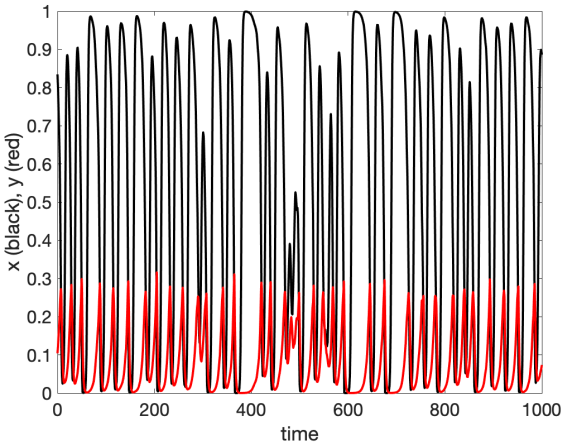

C. $m = 0.7$

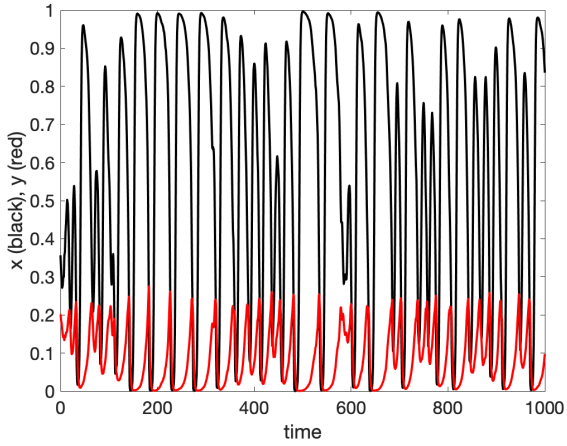

D. $m = 0.75$

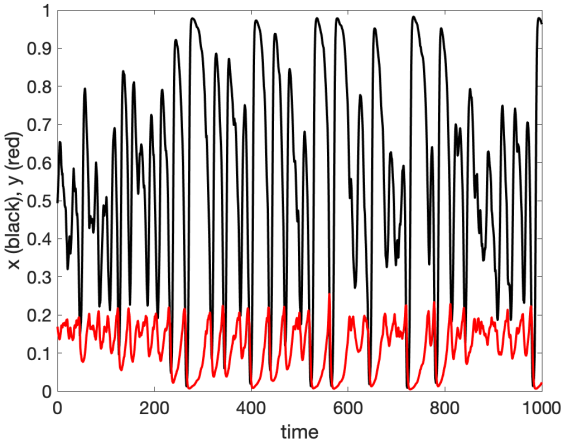

Figure 5

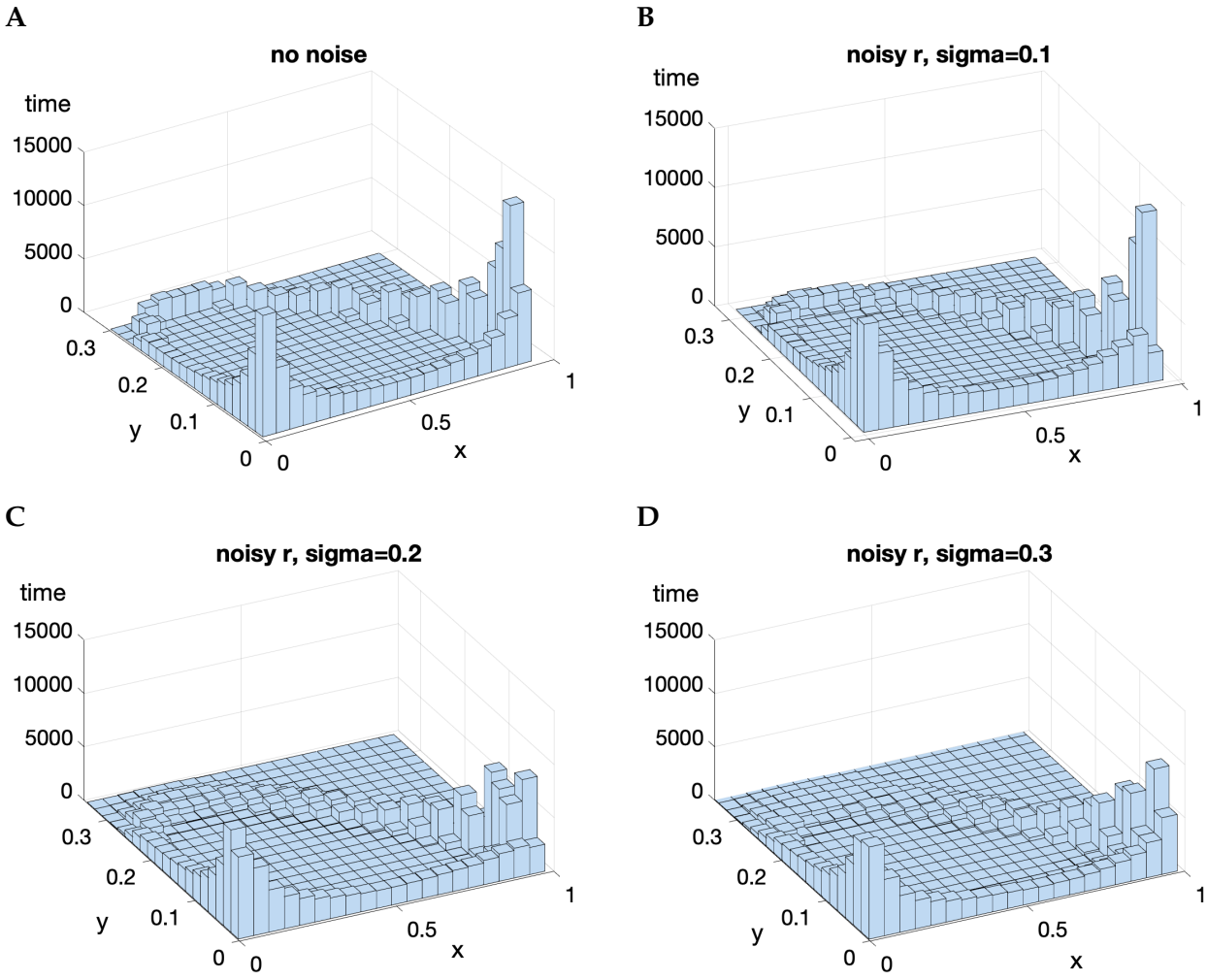
A
no noise
time
15000
10000
5000
0
0.3
0.2
y
0.1
0
0
0.5
1
x
B
noisy r, sigma=0.1
time
15000
10000
5000
0
0.3
0.2
y
0.1
0
0
0.5
1
x
C
noisy r, sigma=0.2
time
15000
10000
5000
0
0.3
0.2
y
0.1
0
0
0.5
1
x
D
noisy r, sigma=0.3
time
15000
10000
5000
0
0.3
0.2
y
0.1
0
0
0.5
1
x

Figure 6

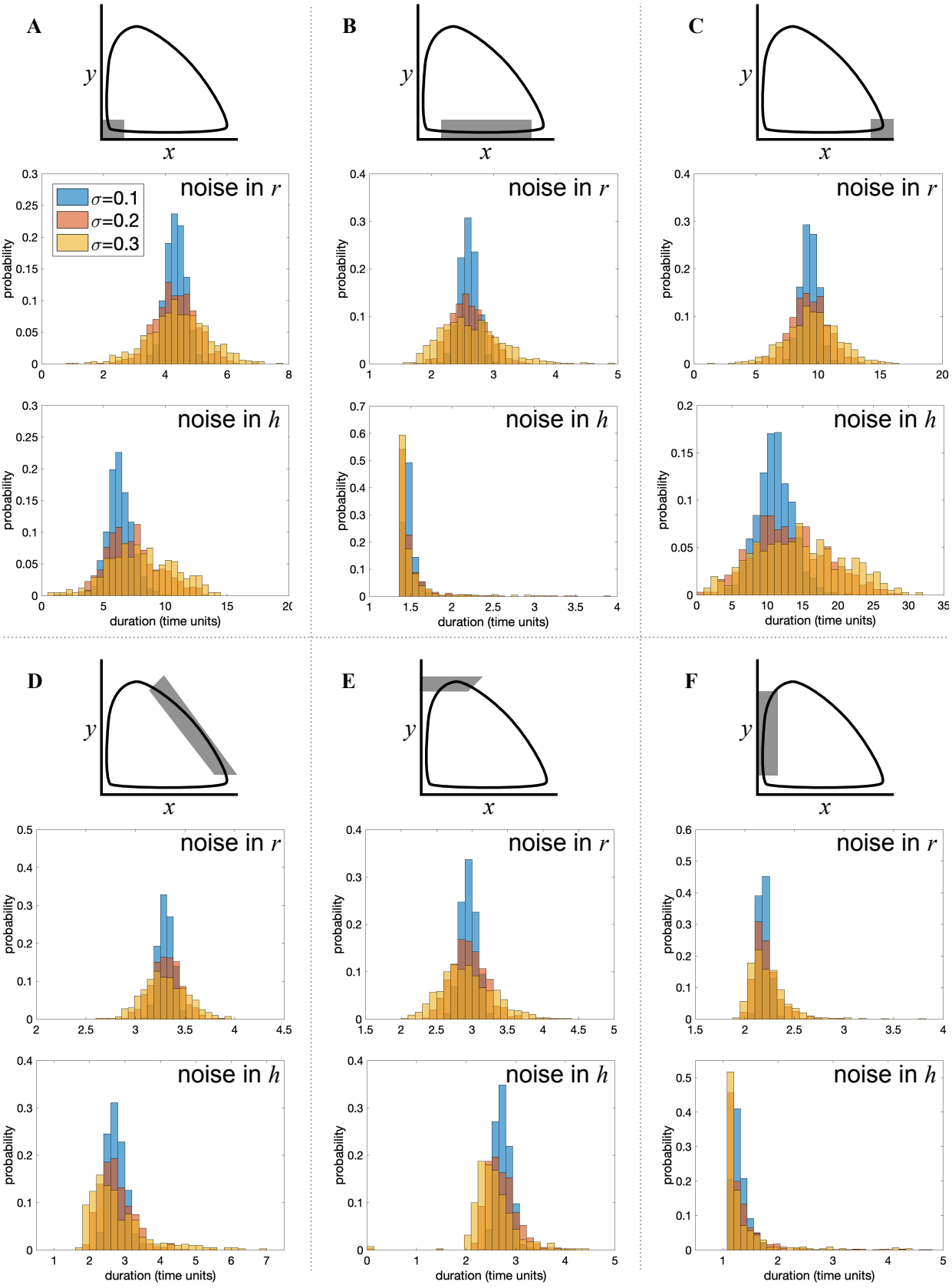
A
B
C
D
E
F
y
x
noise in r
noise in h
σ=0.1
σ=0.2
σ=0.3
probability
duration (time units)

Figure 7

A. Noise in r

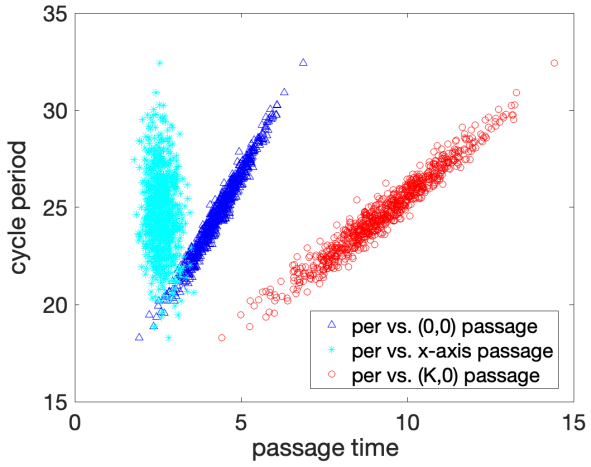

B. Noise in r

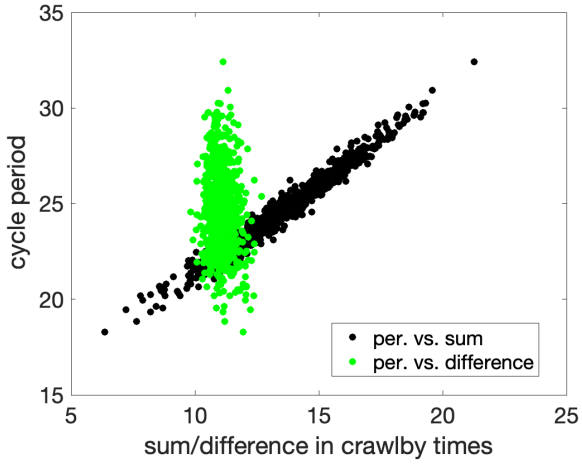

C. Noise in h

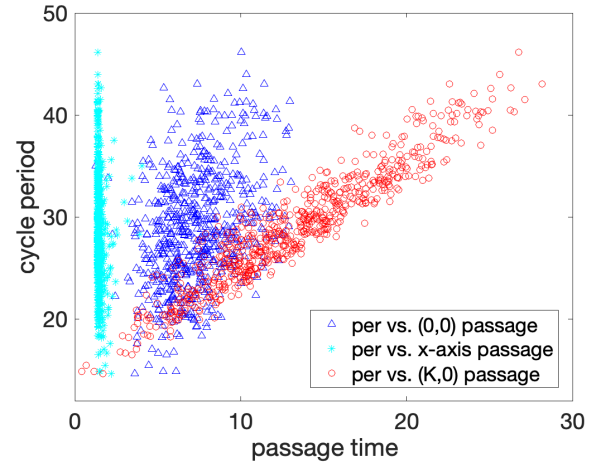

D. Noise in h

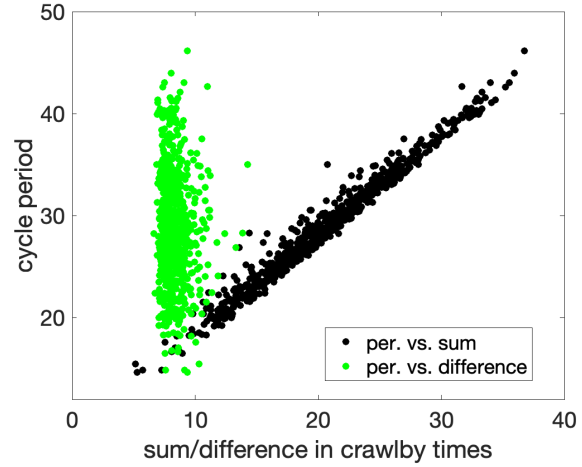

Figure 8

A. Noise in r

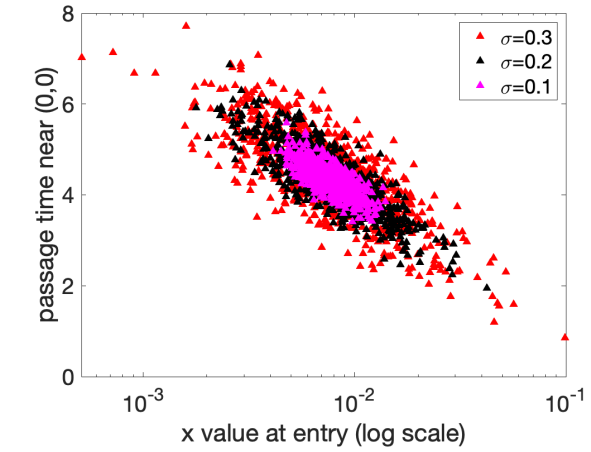

B. Noise in h

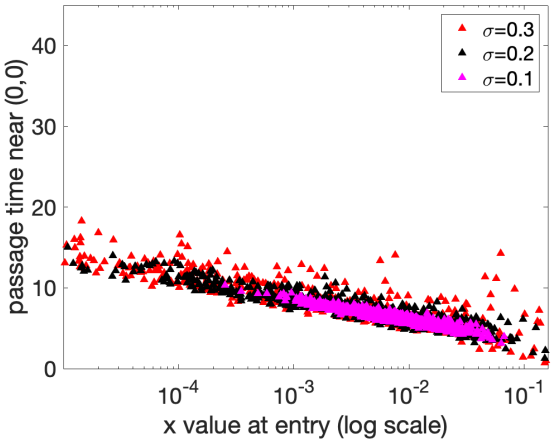

C. Noise in r

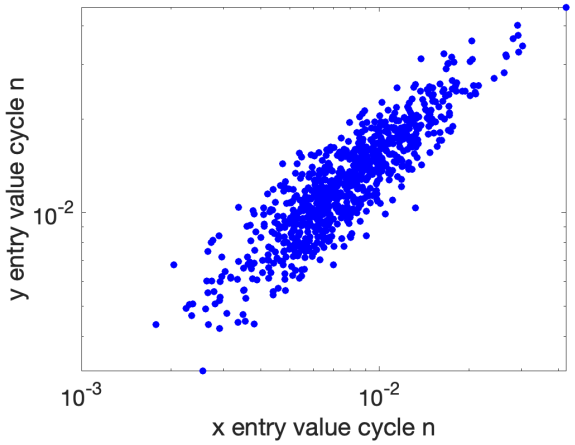

D. Noise in h

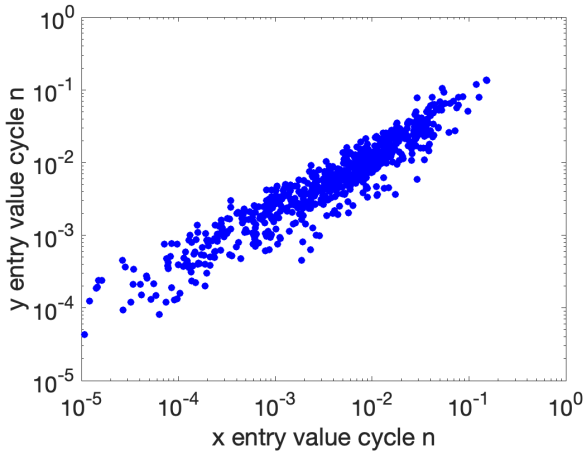

E. Noise in r

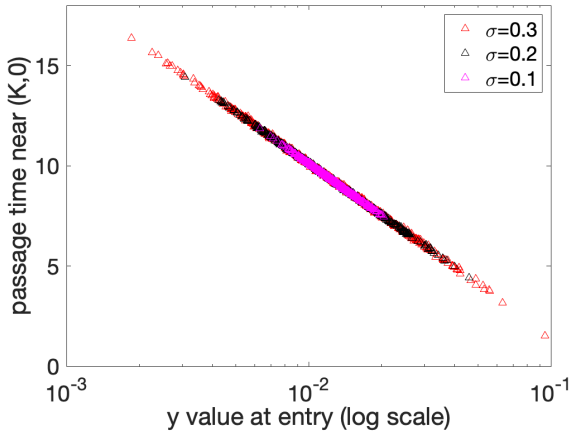

F. Noise in h

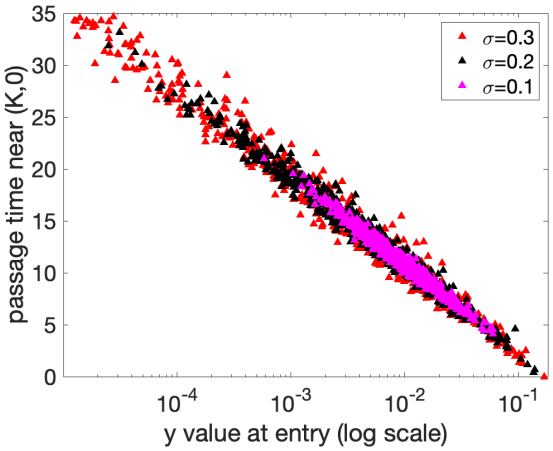

Figure 9

Appendix A: Boundary Layer Analysis

The equations (1) are unfortunately analytically intractable, but the stable limit cycle has segments that are approximately parallel to the x and y axes, which approach closer and closer to the axes as r or h decreases. This allows us to approximate the trajectory via the method of boundary layers, linearizing along the axes.

To do so, we introduce a small, dimensionless parameter ϵ, and substitute $x(t) = \epsilon\xi(t)$ or $y(t) = \epsilon\psi(t)$, as appropriate, into (1). We then take the limit as $\epsilon \to 0$. This is equivalent to focusing on the part of the orbit where the transformed variable(s) are small, and allows us to obtain approximate solutions along the x-axis and y-axis and at the origin. Similarly, letting $x(t) = K + \epsilon\xi(t)$ and $y(t) = \epsilon\psi(t)$, we can approximate the trajectory near the $(K, 0)$ saddle.

We illustrate the method by computing the solution along the y-axis: substituting $x(t) = \epsilon\xi(t)$ into (1) gives

$$\begin{aligned} \epsilon\dot{\xi} &= \epsilon r\xi\left(1 - \frac{\epsilon\xi}{K}\right) - \epsilon\frac{a\xi y}{\epsilon\xi + h} \\ \dot{y} &= \epsilon\frac{ab\xi y}{\epsilon\xi + h} - my. \end{aligned} \tag{A1}$$

In the limit as $\epsilon \to 0$, these equations simplify to

$$\begin{aligned} \dot{\xi} &= \left(r - \frac{ay}{h}\right)\xi \\ \dot{y} &= -my, \end{aligned} \tag{A2}$$

which may be solved to yield $y(t) = y(0)e^{-mt}$ and $\xi(t) = \xi(0)e^{rt - \frac{ay(0)}{mh}(1-e^{-mt})}$, where $y(0)$ and $x(0) = \epsilon\xi(0)$ are the (unspecified) point of entry into a neighborhood of the y-axis. We may also return to the original variables, taking $x(t) = \epsilon\xi(t) = x(0)e^{rt - \frac{ay(0)}{mh}(1-e^{-mt})}$.

When h is allowed to vary stochastically according to equation (2), we need to modify our solution to (A2) to account for the fact that h is a (random) function of time, giving us

$$x(t) = x(0)e^{rt - ay(0)\int_0^t \frac{e^{-mu}}{h(u)}\,du}. \tag{A3}$$

Proceeding similarly, we can obtain approximate local solutions for stochastically varying r

or h, which we summarize in Table A1.

Comparing the solutions along the y-axis for varying r *vs.* varying h gives some intuition for the greater impact of noise in the latter: in this region, the noise enters as $\frac{1}{h}$, whereas h itself fluctuates about a mean of $\bar{h} = 0.15$, and thus will regularly approach values very close to 0. If this happens near the y-axis, $x(t)$, which is proportional to $e^{-\int_0^t \frac{e^{-mu}}{h(u)}\,du}$, can become quite small. This can cause the perturbed trajectory to make a very close approach to the unstable node at the origin and the consequent slow-down of the passage. By contrast, in the same region, noise in r enters linearly, and only a rare, large fluctuation in r will cause the trajectory to have a similar excursion towards the crawlby region near the origin.

Table A1. Linearized solutions for the model defined by equations (1) and (2) in different regions of the phase space.

noise site	region	$x(t)$	$y(t)$
r	origin	$x(0)e^{\int_0^t r(u)\,du}$	$y(0)e^{-mt}$
r	$(K,0)$	$K+(x(0)-K)e^{-\int_0^t r(u)\,du}$ $+\dfrac{ay(0)}{1+h}\displaystyle\int_0^t e^{-\int_s^t r(u)\,du+\left(\frac{ab}{1+h}-m\right)s}\,ds$	$y(0)e^{\left(\frac{ab}{1+h}-m\right)t}$
r	x-axis	$\dfrac{x(0)}{x(0)+(1-x(0))e^{-\int_0^t r(u)\,du}}$	$y(0)e^{abx(0)\int_0^t \frac{1}{x(0)(1+h)+h(1-x(0))e^{-\int_0^u r(v)\,dv}}\,du-mt}$
r	y-axis	$x(0)e^{\int_0^t r(u)\,du-\frac{ay(0)}{mh}(1-e^{-mt})}$	$y(0)e^{-mt}$
h	origin	$x(0)e^{rt}$	$y(0)e^{-mt}$
h	$(K,0)$	$K+(x(0)-K)e^{-rt}+\dfrac{y(0)}{b}e^{ab\int_0^t \frac{1}{1+h(u)}\,du-mt}$ $+\dfrac{y(0)(r-m)}{b}e^{-rt}\displaystyle\int_0^t e^{ab\int_0^s \frac{1}{1+h(u)}\,du+(r-m)s}\,ds$	$y(0)e^{ab\int_0^t \frac{1}{1+h(u)}\,du-mt}$
h	x-axis	$\dfrac{x(0)}{x(0)+(1-x(0))e^{-rt}}$	$y(0)e^{abx(0)\int_0^t \frac{1}{x(0)(1+h(u))+h(u)(1-x(0))e^{-ru}}\,du-mt}$
h	y-axis	$x(0)e^{rt-ay(0)\int_0^t \frac{e^{-mu}}{h(u)}\,du}$	$y(0)e^{-mt}$

Appendix B: Supplemental numerical information and figures

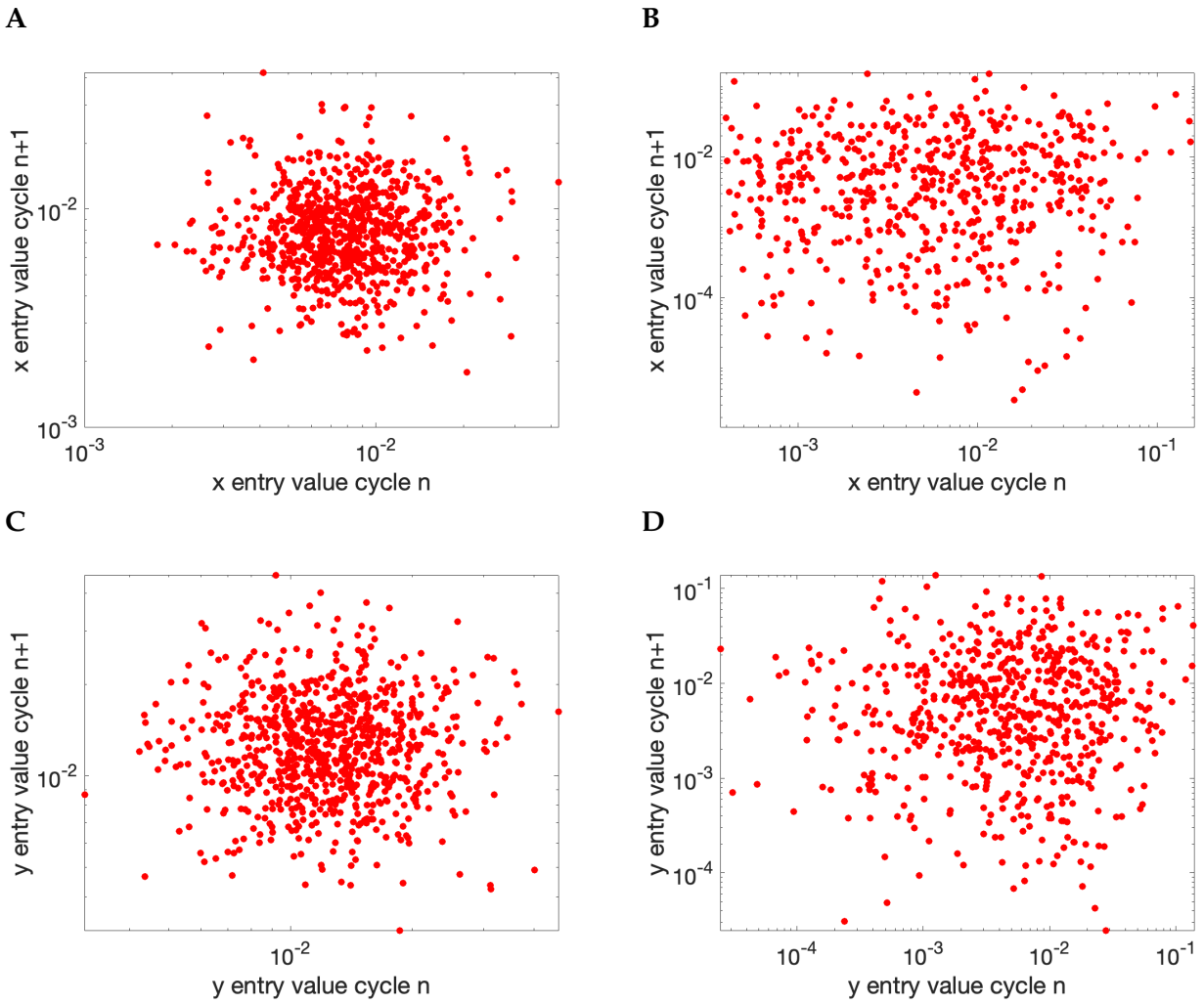

Figure B1. Independence from one cycle to the next of the population densities upon entry into the neighborhoods of the saddles. The stochastic parameter is prey growth rate, r, in **A,C** and predator's prey handling time, h, in **B,D**. **A-B** show the lack of a correlation between prey density upon entry into the $(0,0)$ neighborhood, $\ln(x_{0,\text{in}})$, from the n^{th} to the $n+1^{\text{st}}$ cycle. **C-D** show the same for predator density upon entry into the $(K,0)$ neighborhood, $\ln(y_{K,\text{in}})$. In all cases, $\sigma = 0.2$ and axes are on logarithmic scales. Note that results in **C** include some values of x_{n+1} below the extinction cutoff of 10^{-5}; these were not used in any of the duration calculations discussed in the main text.

Table B1. Entry and exit sections used to define our phase space regions.

noise site	region	entry boundary	exit boundary
h	origin	$y = 0.12$	$x = 0.2$
h	x-axis	$x = 0.2$	$x = 0.5$
h	$(K, 0)$	$x = 0.5$	$y = 0.15$
h	unstable manifold	$y = 0.15$	$y = x - 0.2$
h	y-nullcline	$y = x - 0.2$	$y = 0.23$
h	y-axis	$y = 0.23$	$y = 0.12$
r	origin	$y = 0.07$	$x = 0.12$
r	x-axis	$x = 0.12$	$x = 0.6$
r	$(K, 0)$	$x = 0.6$	$y = 0.13$
r	unstable manifold	$y = 0.13$	$y = 0.55x$
r	y-nullcline	$y = 0.55x$	$y = 0.22$
r	y-axis	$y = 0.22$	$y = 0.07$

These values were used for all results except cases 6-9 in Table 2, for which sections were slightly adjusted to reflect altered orbit paths.

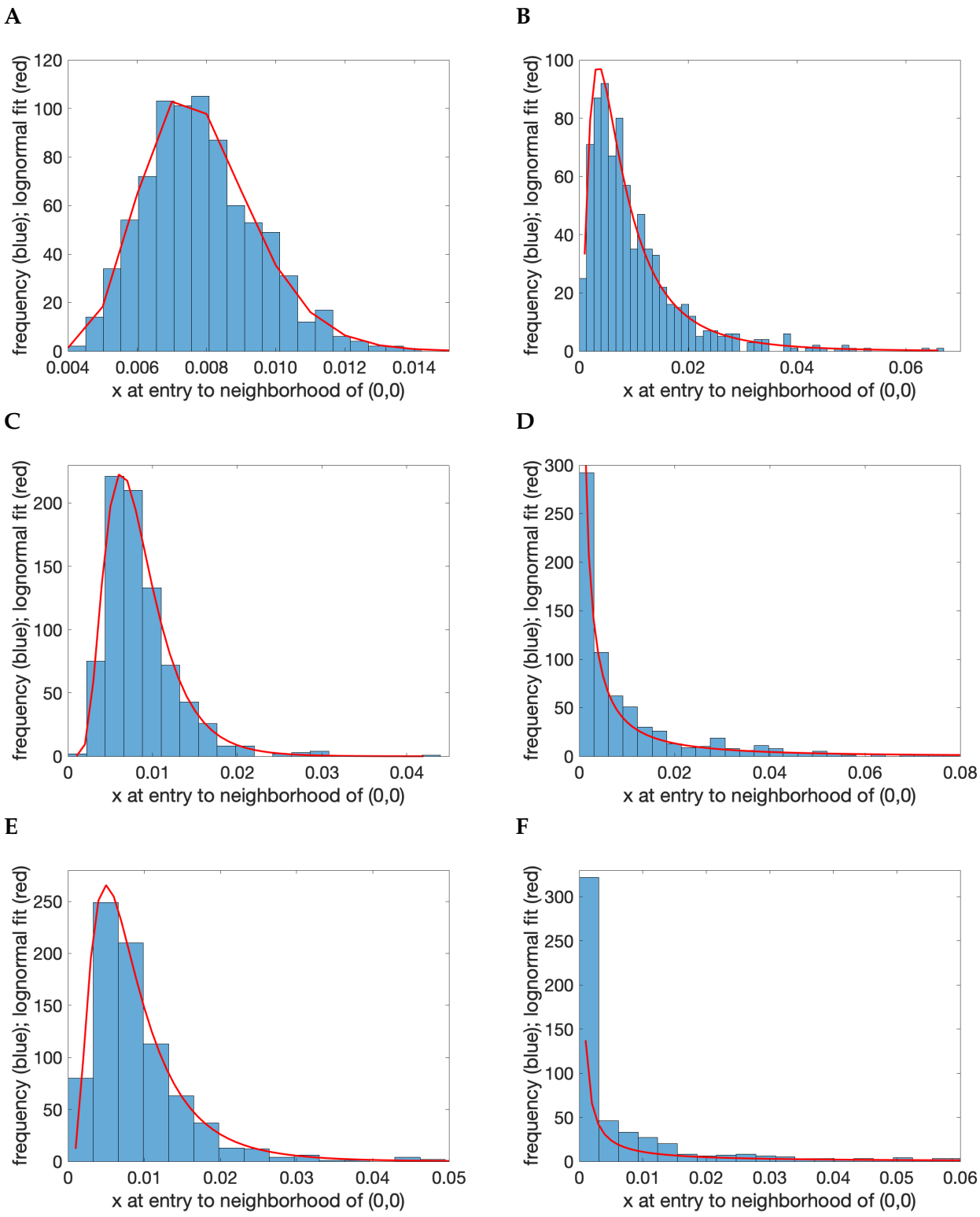

Figure B2. Distributions of prey densities, $\ln(x_{0,\text{in}})$, at crossing of a Poincaré section of constant $y = y_{0,\text{in}}$, which marks entry into the neighborhood of $(0,0)$. **A,B**: $\sigma = 0.1$, **C,D**: $\sigma = 0.2$, **E,F**: $\sigma = 0.3$. The noisy parameter is r in the left panels (with $y_{0,\text{in}} = 0.07$) and h in the right panels (with $y_{0,\text{in}} = 0.12$). In each panel, the red curve shows the best lognormal fit to each distribution.

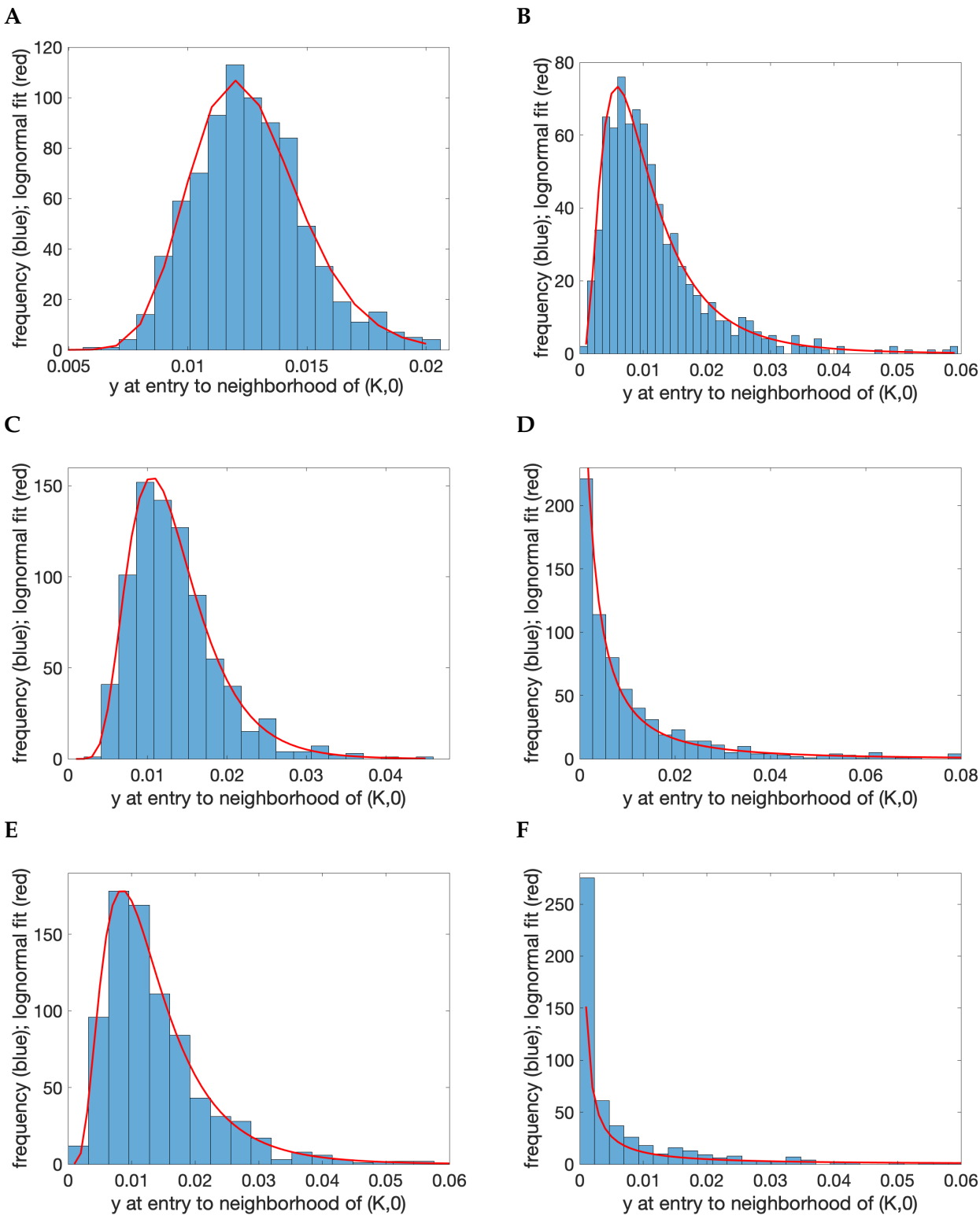

Figure B3. Distributions of predator densities, $y_{K,\text{in}}$, at crossing of a Poincaré section of constant $x = x_{K,\text{in}}$, marking entry into the neighborhood of $(K, 0)$. **A,B**: $\sigma = 0.1$, **C,D**: $\sigma = 0.2$, **E,F**: $\sigma = 0.3$. The noisy parameter is r in the left panels (with $x_{K,\text{in}} = 0.6$) and h in the right panels (with $x_{K,\text{in}} = 0.5$). In each panel, the red curve shows the best lognormal fit to each distribution.